Journal of Magnetic Resonance 213 (2011) 46–57

Contents lists available at SciVerse ScienceDirect

Journal of Magnetic Resonance

journal homepage: www.elsevier.com/locate/jmr

Theory of mirrored time domain sampling for NMR spectroscopy

Arindam Ghosh [1], Yibing Wu [2], Yunfen He, Thomas Szyperski *

Department of Chemistry, The State University of New York at Buffalo, Buffalo, NY 14260, United States

ARTICLE INFO

Article history:
Received 5 May 2011
Revised 2 August 2011
Available online 5 September 2011

Keywords:
NMR spectroscopy
Phase-sensitive
Quadrature detection
Pure absorption mode
Clean absorption mode
Mirrored time domain sampling

ABSTRACT

A generalized theory is presented for novel mirrored hypercomplex time domain sampling (MHS) of NMR spectra. It is the salient new feature of MHS that two interferograms are acquired with different directionality of time evolution, that is, one is sampled forward from time $t = 0$ to the maximal evolution time t_{max}, while the second is sampled backward from $t = 0$ to $-t_{max}$. The sampling can be accomplished in a (semi) constant time or non constant-time manner. Subsequently, the two interferograms are linearly combined to yield a complex time domain signal. The manifold of MHS schemes considered here is defined by arbitrary settings of sampling phases ('primary phase shifts') and amplitudes of the two interferograms. It is shown that, for any two given primary phase shifts, the addition theorems of trigonometric functions yield the unique linear combination required to form the complex signal. In the framework of clean absorption mode (CAM) acquisition of NMR spectra being devoid of residual dispersive signal components, 'secondary phase shifts' represent time domain phase errors which are to be eliminated. In contrast, such secondary phase shifts may be introduced by experimental design in order to encode additional NMR parameters, a new class of NMR experiments proposed here. For generalization, it is further considered that secondary phase shifts may depend on primary phase shifts and/or sampling directionality. In order to compare with MHS theory, a correspondingly generalized theory is derived for widely used hypercomplex ('States') sampling (HS). With generalized theory it is shown, first, that previously introduced 'canonical' schemes, characterized by primary phases being multiples of $\pi/4$, afford maximal intensity of the desired absorptive signals in the absence of secondary phase shifts, and second, how primary phases can be adjusted to maximize the signal intensity provided that the secondary phase shifts are known. Third, it is demonstrated that theory enables one to accurately measure secondary phase shifts and amplitude imbalances. Application to constant time 2D [^{13}C, ^{1}H]-HSQC spectra recorded for a protein sample with canonical MHS/HS schemes showed that accurate CAM data acquisition can be readily implemented on modern spectrometers for experiments based on through-bond polarization transfer. Fourth, when moderate variations of secondary phase shifts with primary phase shift and/or sampling directionality are encountered, generalized theory allowed comparison of the robustness of different MHS/HS schemes for CAM data acquisition, and thus to identify the scheme best suited to suppress dispersive peak components and quadrature image peaks. Moreover, it is shown that for spectra acquired with several indirect evolution periods, the best suited scheme can be identified independently for each of the periods.

1. Introduction

The sampling of the time evolution of the spin density matrix is pivotal for nuclear magnetic resonance (NMR) spectroscopy [1], which is among the most powerful analytical tools widely used in natural sciences and engineering [2]. In particular, multidimensional NMR experiments enable one to directly correlate several NMR parameters. The majority of N dimensional experiments

Abbreviations: CAM, clean absorption mode; FT, Fourier Transform; GFT, G-matrix Fourier Transform; HS, hypercomplex sampling; HSQC, heteronuclear single quantum coherence; DHS, dual hypercomplex sampling; DMHS, dual mirrored hypercomplex sampling; FOM, figure of merit; INEPT, insensitive nuclei enhanced by polarization transfer; MHS, mirrored hypercomplex sampling; RD, reduced dimensionality; r.f., radio-frequency; TOCSY, total correlation spectroscopy; TPPI, time proportional phase incrementation.

* Corresponding author. Fax: +1 716 645 6963.
E-mail address: szypersk@buffalo.edu (T. Szyperski).
[1] Present address: National Institute of Science Education and Research, Bhubaneswar 751 005, India.
[2] Present address: Department of Biochemistry and Biophysics, School of Medicine, University of Pennsylvania, Philadelphia, PA 19104, United States.

1090-7807/$ - see front matter © 2011 Elsevier Inc. All rights reserved.
doi:10.1016/j.jmr.2011.08.037

($N > 1$) correlate N chemical shifts, of which $N - 1$ are measured in indirect dimensions [3]. In 'Fourier Transform (FT) NMR', the indirect dimensions are sampled in the time domain before suitable transformation (*e.g.*, a FT) generates the frequency domain presentation of the spectrum which is then analyzed. The specific protocol employed for sampling the time domain of an indirect dimension is critical to achieve high spectral resolution [1] and advances of sampling protocols thus meet with a wide demand. It is most desirable to sample for 'pure absorption mode': for time domain signals decaying mono-exponentially this yields Lorentzian line shapes in the frequency domain, and peaks located at frequency Ω_0 decay proportional to $1/(\Omega_0 - \Omega)^2$. Pure absorption mode data acquisition aims at avoiding dispersive peaks (or dispersive peak components superimposed on the desired absorptive signals) because those decay only slowly, *i.e.*, proportional to $1/(\Omega_0 - \Omega)$.

Pure absorption mode time domain data acquisition can be accomplished by using two distinctly different approaches, that is, by 'hypercomplex sampling' (HS) [1,4], which can be also be described by the use of quarternions [5], or by 'time proportional phase incrementation' (TPPI) [6–10]. HS relies on separately sampling both the cosine and the sine modulation of the *amplitude* of the directly detected NMR signal with the evolution of chemical shifts in an indirect dimension. The resulting two interferograms are combined to form a complex time domain signal, and subsequent *complex* FT, along with proper adjustment of phases ('zero'- and 'first order-'phase corrections), yields the desired absorptive signals in the frequency domain. In contrast, when using TPPI, only one interferogram is acquired, where (a) the increment of the delay representing the indirect evolution period is reduced to half of what is used for HS (*i.e.*, the spectral width is doubled), and (b) the phase of the radio-frequency (r.f.) pulse generating transverse magnetization is incremented along with the incrementation of the indirect evolution period, so that the apparent carrier position is shifted to the edge of the spectral range. Cosine (or 'real') FT, along with proper adjustment of phases and discarding quadrature image peaks, yields the desired absorptive signals in the frequency domain. The TPPI approach requires that r.f. pulse phases can be set very accurately, since errors in r.f. pulse phases translate into systematic errors of the measured chemical shifts. Moreover, HS and TPPI based pure absorption mode data acquisition differ in how peaks located outside of the chosen spectral range are 'folded back' into the spectrum [3]. Nowadays, the majority of multidimensional NMR experiments are acquired using HS.

This is also due to the fact that after the seminal work of States et al. [4] on HS was published, a variety of data acquisition schemes were introduced in which first two interferograms are acquired that encode chemical shifts in the directly detected signals by *phase modulation* in the two opposite senses of rotations (note that such approaches cannot be implemented when using TPPI since only a single interferogram is acquired). These interferograms are then linearly combined to construct the desired cosine and sine *amplitude* modulations. Among those schemes are (i) the acquisition of 'echo'/'anti-echo' interferograms by use of pulsed B-field gradients [11,12], (ii) sensitivity enhancement schemes for NMR experiments correlating chemical shifts of two nuclei which exhibit a comparably large one-bond scalar coupling used for polarization transfer [13], and (iii) approaches combining (i) and (ii) [14,15].

Very recently, mirrored hypercomplex (MHS) time domain sampling [16] was introduced for clean absorption mode (CAM) NMR data acquisition of (semi) constant time [3] as well as non constant-time [1,3] experiments [16]. This novel approach aims at removing residual dispersive peak components that cannot be eliminated by zero- or first-order phase correction, or occur in G-matrix FT (GFT) [17] based projection NMR [18–27], where phase errors of jointly sampled chemical shifts are entangled and phase corrections cannot be applied for individual evolution periods. The elimination of such residual dispersive peak components is important because they (i) increase spectral overlap, and (ii) shift the maxima of peaks, thereby reducing the accuracy of chemical shift measurements [16]. As a distinct new feature, the two interferograms for construction of the complex time domain signal are acquired with different directionality of the time evolution, that is, one interferogram is sampled forward from time $t = 0$ to the maximal evolution time t_{max}, while the second one is sampled backward from $t = 0$ to $-t_{max}$. Note that Nagayama [28] published an approach for *processing* of 2D spectra which relies on (i) linearly combining the interferograms obtained by HS [4] to generate two interferograms encoding chemical shifts in the directly detected signals by *phase modulation* in the two opposite senses of rotations, (ii) inverting the order of the data points of the one of the phase modulated spectra so that they are sorted from $t = t_{max}$ to 0 ('time reversal') and forming the complex conjugate (*i.e.*, 'frequency inversion'), and (iii) adding the two thus obtained phase modulated spectra with the aim to create 2D spectra devoid of mixed phases. However, it can be shown that this approach is not generally applicable. In particular, the approach can hardly be employed for constant time evolution periods, or when t_{max} is much shorter than the transverse relaxation time T_2 of the evolving spin (see Supplementary Material). Moreover, in contrast to this approach for data processing, MHS represents an *acquisition* technique relying on interferograms which are sampled from $t = 0$ to $-t_{max}$ (see above). As a result, CAM data acquisition is based on distinct considerations for its implementation, as is discussed in the following.

For efficient CAM data acquisition, it is crucial to design and set up a given experiment such that first and second order phase corrections are zero. This is because CAM data acquisition eliminates *all* phase shifts independent of their origin and at the expense of signal intensity [16]: zero order phase shifts (being the same for all signals) and first order phase shifts (being linearly correlated with chemical shifts) are eliminated as well as residual phase errors which are not linearly correlated with chemical shifts. To exemplify this feature of CAM data acquisition, we previously published [16] cross sections taken from non constant time 2D [^{13}C, ^{1}H]-HSQC [3] spectra recorded for a protein sample employing HS/MHS schemes with delayed acquisition, resulting in 108° first order phase corrections over the ^{13}C spectral range (see Supporting Information of [16], Section V, p. 43). Taken together, elimination of phase shifts in CAM shall preferably [16] be limited to phase errors which *cannot* be eliminated (i) by experimental design aiming at pure phases and (ii) by avoiding delayed acquisition [3]. Importantly, it has been shown [16] that (i) for phase errors up to about ±15° the resulting loss of signal intensity is negligible, *i.e.*, less than about 4%, and that (ii) the 'sampling demand' is not increased whenever quadrature image peaks are within the noise floor or fall in otherwise empty spectral regions, or when dual MHS is combined with (at least) a 2-step phase cycle required anyways for artifact suppression. It has also been shown that CAM data acquisition can be implemented for both (semi) constant time and non constant time evolution periods [16]. For (semi) constant time evolution periods, the 180° r.f. pulse refocusing chemical shift evolution is simply shifted in opposite directions to enable opposite sampling directionality. Non constant time sampling, which likewise requires that a 180° r.f. pulse is applied [16], can be rationalized as the limit of semi constant time sampling in which the delay between the 180° pulse and the 90° r.f. pulses at the beginning or the end of the evolution period is set to zero (for a product operator description see Section III of the Supporting Information of [16]).

A given HS/MHS scheme can be characterized by defining the two interferograms which yield the complex time domain signal required for pure absorption mode acquisition. Previously [16] we defined, for a given chemical shift α, an interferogram by the equation

$c_{\pm n} := \cos(\pm\alpha t + n\pi/4 + \Phi)$, where '±' indicates forward ('+') *or* backward ('−') time domain sampling, $n = 0, 1, 2$ or 3 defines as $n\pi/4$ the 'primary phase shift', *i.e.* the difference between the phases of the two r.f. pulses used to first generate transverse magnetization at the start of the chemical shift evolution period and then to transfer magnetization at the end of the chemical shift evolution period. In this paper, such sampling schemes with primary phases being multiples of $\pi/4$ will be referred to as the 'canonical' schemes. Φ denotes a 'secondary phase shift' which represents, in the framework of CAM data acquisition, a phase error. Alternatively, novel experiments are conceivable in which the secondary phase shift encodes an NMR parameter. In this case, the employment of MHS does not aim at eliminating the phase shift but at enabling its accurate measurement by integrating purely absorptive peaks and quadrature image peaks to obtain the value of the parameter.

The two interferograms chosen for a given HS/MHS scheme form an interferogram vector **C**, which in turn is multiplied by a matrix **D** to generate the linear combinations of the interferograms required to construct the complex time domain signal [16]. MHS with $\mathbf{C} = (c_{+1}, c_{-1})$ or $\mathbf{C} = (c_{+0}, c_{-2})$ offers the unique opportunity of transferring a dispersive signal component, which would arise from a secondary phase shift when employing HS ['States' sampling [4]; $\mathbf{C} = (c_{+0}, c_{+2})$], into a quadrature image peak being, respectively, purely absorptive or dispersive [16]. Furthermore, we showed that use of dual MHS (DMHS) with $n = 1$ and $n = 3$ and recently introduced dual HS (DHS) [16] or dual TPPI [10] with forward and backward sampling, along with subsequent addition of the resulting spectra, enables one to eliminate signals arising from the presence of the phase errors [16]. This, however, relies on the time domain signal amplitude and the phase errors being independent of primary phase shifts and time domain sampling direction. Note that the name 'MHS' chosen here differs from the previously introduced name 'phase-shifted mirrored sampling' (PMS). This is because in the framework of a generalized theory arbitrary shifting of primary phases is implicit, and the name 'MHS' emphasizes that such sampling schemes belong to the class of hypercomplex as opposed to TPPI sampling schemes.

We present here a generalized theory of MHS, DMHS and, for comparison, of HS and DHS. The manifold of considered schemes is defined by arbitrary settings of primary phase shifts and amplitudes of the two interferograms. Moreover, the theories encompass cases where secondary phase shifts are dependent on primary phase shifts and/or time domain sampling directionality.

2. Theory

For deriving the generalized MHS and HS theory [16], the following definitions are chosen to characterize the two interferograms (Table 1) used to construct the desired complex time domain signal. A given sampling scheme is defined by two primary phase shifts $\psi \in [0, 2\pi[$ and $\psi + \delta \in [0, 2\pi[$ (the open intervals exclude 2π which is equal to a 0° shift) and the directionality of time domain sampling. Hence, each of the two interferograms can be defined by

$$c_{\psi+\delta}(\pm t) := I^{\pm}_{\psi+\delta} \cos(\psi + \delta \pm \alpha t + \Phi^{\pm}_{\psi+\delta}) \quad (1)$$

where $\delta = 0$ for the first interferogram and $\delta \in [0, 2\pi[$ represents the difference between the primary phase shift of the second and first interferogram, and '+' or '−' in '±' applies for forward and backward sampling, respectively. Φ and I represent the secondary phase shift and relative time domain signal amplitude, which are in the following assumed to be different for different detected signals and may depend on the sampling direction (indicated by superscript '±') and/or the primary phase shift (indicated by subscript '$\psi + \delta$'). The fact that the primary phases can be set arbitrarily implies that a

Table 1
Survey of canonical NMR time domain sampling schemes.[a]

Sampling scheme	ψ	δ	p	q	Interferograms[b]
i. Mirrored hypercomplex sampling (MHS)					
$\pi4,\pi/4$ – MHS	$\pi/4$	0	1	–	$c_{\frac{\pi}{4}}(t) \equiv c_{+1}$
			–	1	$c_{\frac{\pi}{4}}(-t) \equiv c_{-1}$
$3\pi4,3\pi/4$ – MHS	$3\pi/4$	0	3	–	$c_{\frac{3\pi}{4}}(t) \equiv c_{+3}$
			–	3	$c_{\frac{3\pi}{4}}(-t) \equiv c_{-3}$
$0,\pi/2$ – MHS	0	$\pi2$	0	–	$c_0(t) \equiv c_{+0}$
			–	2	$c_{\frac{\pi}{2}}(-t) \equiv c_{-2}$
$\pi/2,3\pi/2$ – MHS	$\pi/2$	$3\pi2$	2	–	$c_{\frac{\pi}{2}}(t) \equiv c_{+2}$
			–	0	$c_0(-t) \equiv c_{-0}$
ii. Hypercomplex sampling (HS)					
Forward HS	0	$\pi2$	0	–	$c_0(t) \equiv c_{+0}(t)$
			–	2	$c_{\frac{\pi}{2}}(t) \equiv c_{+2}$
Backward HS	0	$\pi2$	0	–	$c_0(-t) \equiv c_{-0}(-t)$
			–	2	$c_{\frac{\pi}{2}}(-t) \equiv c_{-2}(-t)$

[a] p and q define the primary phase shifts according to $\psi = p\pi/4$ and $\psi + \delta = q\pi/4$.
[b] For comparison, interferograms are represented using both the nomenclature previously adopted for CAM data acquisition [16] (on the right) and the nomenclature required for the generalized formalism presented in this paper (on the left). Accordingly, the two interferograms required to construct the complex time domain signal are represented by $(c_{\psi}(\pm t), c_{\psi+\delta}(\pm t))$ in the nomenclature of this paper and by $(c_{\pm p}, c_{\pm q})$ in the shorter nomenclature previously introduced for canonical schemes [16].

D-matrix [16] for linear combination of the interferograms needs to be derived which is a function of the two primary phases.

As for the canonical sampling schemes introduced previously [16], the manifold of generalized schemes represented by Eq. (1) is classified according to the *directionality* of time domain sampling: for MHS one interferogram is sampled forward and the other backward, and for HS both interferograms are sampled in the same direction (both forward or both backward). Notably, the generalized theory of HS enables one to connect the concepts presented here to the widely used canonical HS introduced by States et al. [4]. For the sake of conciseness, generalized HS theory is provided as Supplementary Material.

2.1. Mirrored hypercomplex sampling (MHS)

A generalized theoretical description of MHS shall be established by pursuing the following steps: (1) definition of the interferogram **C**-vector; (2) derivation of the corresponding **D**-matrix for linearly combining the interferograms; (3) proof that the intensities of the desired absorptive signals scale with the determinant of **D** and that canonical MHS schemes, which are characterized by primary shifts being multiples of $\pi/4$, provide maximal signal intensity in the absence of secondary phase shifts and amplitude imbalances; (4) calculation of the complex time domain signal obtained when employing generalized MHS and **D**-matrix; (5) derivation of a condition for maximal intensity of desired absorptive signals considering the presence of secondary phase shifts, but in the absence of amplitude imbalances; (6) derivation of the time domain signal obtained when employing generalized canonical MHS; and (7) surveying implications of MHS and **D**-matrix transformation for the subsequent transformation into frequency domain data. For illustration, simulated spectra obtained with generalized MHS are shown in Fig. 2 and referred to in the following.

1. Definition of **C**-vector.

It is the defining feature of MHS that the two interferograms used to construct the complex time domain signal are sampled in *different* directions, that is, the first one along $+t$ and the second one along $-t$, thereby yielding with definitions introduced for Eq. (1):

$$\mathbf{C} = \begin{bmatrix} I^{+}_{\psi} c_{\psi}(t) \\ I^{-}_{\psi+\delta} c_{\psi+\delta}(-t) \end{bmatrix} = \begin{bmatrix} I^{+}_{\psi} \cos(\psi + \alpha t + \Phi^{+}_{\psi}) \\ I^{-}_{\psi+\delta} \cos(\psi + \delta - \alpha t + \Phi^{-}_{\psi+\delta}) \end{bmatrix} \quad (2)$$

2. Derivation of **D**-matrix.

In order to form linear combinations of the two **C**-vector interferograms [Eq. (1)] yielding the desired pure cosine and sine modulations to construct the complex time domain signal, a generalized **D**-matrix is derived, which is a function of the primary phase shifts only. Hence, amplitudes and secondary phase shifts in **C** are set to 1 and 0, respectively. According to the addition theorems of trigonometric function, Eq. (2) yields

$$\begin{aligned} \mathbf{C} &= \begin{bmatrix} c_{\psi}(t) \\ c_{\psi+\delta}(-t) \end{bmatrix} = \begin{bmatrix} \cos(\psi + \alpha t) \\ \cos(\psi + \delta - \alpha t) \end{bmatrix} \\ &= \begin{bmatrix} \cos\psi \cos\alpha t - \sin\psi \sin\alpha t \\ \cos(\psi + \delta)\cos\alpha t + \sin(\psi + \delta)\sin\alpha t \end{bmatrix} \end{aligned} \quad (3)$$

so that the two interferograms can be linearly combined according to:

$$\begin{aligned} &\sin(\psi+\delta)c_{\psi}(t) + \sin\psi c_{\psi+\delta}(-t) = \sin(2\psi+\delta)\cos\alpha t \\ &-\cos(\psi+\delta)c_{\psi}(t) + \cos\psi c_{\psi+\delta}(-t) = \sin(2\psi+\delta)\sin\alpha t \\ &\Longleftrightarrow \begin{bmatrix} \sin(\psi+\delta) & \sin\psi \\ -\cos(\psi+\delta) & \cos\psi \end{bmatrix} \begin{bmatrix} c_{\psi}(t) \\ c_{\psi+\delta}(-t) \end{bmatrix} = \mathbf{D} \begin{bmatrix} c_{\psi}(t) \\ c_{\psi+\delta}(-t) \end{bmatrix} = \sin(2\psi+\delta) \begin{bmatrix} \cos\alpha t \\ \sin\alpha t \end{bmatrix} \end{aligned} \quad (4)$$

where the **D**-matrix thus emerges as

$$\mathbf{D} = \begin{bmatrix} \sin(\psi+\delta) & \sin\psi \\ -\cos(\psi+\delta) & \cos\psi \end{bmatrix}.$$

A pictorial derivation of the **D**-matrix is presented in Fig. 1a–c, where the forward and backward sampled interferograms $c_{\psi}(t)$ and $c_{\psi+\delta}(-t)$ are represented, respectively, by unit vectors $\hat{e}_{-\psi}$ and $\hat{e}_{\psi+\delta}$ with polar angles $-\psi$ and $\psi + \delta$ in the plane spanned by basis vectors representing $\cos\alpha t$ and $\sin\alpha t$. For comparison, the analogous pictorial derivation for HS is presented in Fig. 1d–f.

3. Intensities of complex time domain signal scales with the determinant of **D**.

The area of the parallelogram formed by $\hat{e}_{-\psi}$ and $\hat{e}_{\psi+\delta}$ is given by the determinant of the **D**-matrix:

$$\begin{aligned} \begin{vmatrix} \sin(\psi+\delta) & \sin\psi \\ -\cos(\psi+\delta) & \cos\psi \end{vmatrix} &= \sin(\psi+\delta)\cos\psi + \cos(\psi+\delta)\sin\psi \\ &= \sin(2\psi+\delta) \end{aligned} \quad (5)$$

which is, according to Eq. (4), proportional to the time domain signal amplitude. Hence, signal intensity is maximal for orthogonal vectors $\hat{e}_{-\psi}$ and $\hat{e}_{\psi} + \delta$. This is given if

$$2\psi + \delta = (2n+1)\frac{\pi}{2} \quad n = 0, 1 \quad (6)$$

This condition constrains the two primary phase shifts to the values chosen for previously published canonical MHS [16] [Table 1(i)], and proves that these schemes provide maximal signal intensity in the absence of secondary phase shifts and amplitude imbalances. Any deviation results in a reduction of the intensity of desired absorptive signals. In the limiting case of $2\psi + \delta = 0$, one has that the two vectors $\hat{e}_{-\psi}$ and $\hat{e}_{\psi+\delta}$ are collinear (*i.e.*, det**D** = 0) and such sampling does not afford phase sensitive signal detection [16,29].

4. Complex time domain signal resulting from MHS and **D**-matrix transformation.

With the **D**-matrix of Eq. (4), the complex *time* domain signal $S_{\psi,\delta}(t)$ is then proportional to (see derivation of Eq. (S1) of Section I in the Supplementary Material for intermediate steps of the calculation):

$$\begin{aligned} S_{\psi,\delta}(t) \propto \mathbf{Q}\,\mathbf{D}\,\mathbf{C} &= [1 \quad i] \begin{bmatrix} \sin(\psi+\delta) & \sin\psi \\ -\cos(\psi+\delta) & \cos\psi \end{bmatrix} \begin{bmatrix} I^{+}_{\psi} c_{\psi}(t) \\ I^{-}_{\psi+\delta} c_{\psi+\delta}(-t) \end{bmatrix} \\ &= [1 \quad i] \begin{bmatrix} \sin(\psi+\delta) & \sin\psi \\ -\cos(\psi+\delta) & \cos\psi \end{bmatrix} \\ &\times \begin{bmatrix} I^{+}_{\psi}\left(\cos\psi\cos\left(\alpha t + \Phi^{+}_{\psi}\right) - \sin\psi\sin\left(\alpha t + \Phi^{+}_{\psi}\right)\right) \\ I^{-}_{\psi+\delta}\left(\cos(\psi+\delta)\cos\left(\alpha t - \Phi^{-}_{\psi+\delta}\right) + \sin(\psi+\delta)\sin\left(\alpha t - \Phi^{-}_{\psi+\delta}\right)\right) \end{bmatrix} \\ &= \frac{1}{2}\left(I^{+}_{\psi}\sin\left(2\psi+\delta+\Phi^{+}_{\psi}\right) + I^{-}_{\psi+\delta}\sin\left(2\psi+\delta+\Phi^{-}_{\psi+\delta}\right)\right)e^{i\alpha t} \\ &\quad -\frac{1}{2}\left(I^{+}_{\psi}\cos\left(2\psi+\delta+\Phi^{+}_{\psi}\right) - I^{-}_{\psi+\delta}\cos\left(2\psi+\delta+\Phi^{-}_{\psi+\delta}\right)\right)e^{i\frac{\pi}{2}}e^{i\alpha t} \\ &\quad +\frac{1}{2}\left(I^{+}_{\psi}\sin\left(\delta-\Phi^{+}_{\psi}\right) - I^{-}_{\psi+\delta}\sin\left(\delta+\Phi^{-}_{\psi+\delta}\right)\right)e^{-i\alpha t} \\ &\quad -\frac{1}{2}\left(I^{+}_{\psi}\cos\left(\delta-\Phi^{+}_{\psi}\right) - I^{-}_{\psi+\delta}\cos\left(\delta+\Phi^{-}_{\psi+\delta}\right)\right)e^{i\frac{\pi}{2}}e^{-i\alpha t} \\ &= \lambda^{A+}_{MHS}e^{i\alpha t} + \lambda^{D+}_{MHS}e^{i\frac{\pi}{2}}e^{i\alpha t} + \lambda^{A-}_{MHS}e^{-i\alpha t} + \lambda^{D-}_{MHS}e^{i\frac{\pi}{2}}e^{-i\alpha t} \end{aligned} \quad (7)$$

where **Q** = [1 i] and the λ-coefficients represent [16], respectively, the relative intensities of absorptive ($A+$) and dispersive ($D+$) signal components located at $+\alpha$ in the frequency domain, as well as the relative intensities of absorptive ($A-$) and dispersive ($D-$) quadrature signal components located at $-\alpha$ in the frequency domain.

5. Condition for maximal signal intensity in the absence of amplitude imbalances.

A condition for maximal signal intensity shall be derived when MHS is employed for CAM data acquisition in the presence of secondary phase shifts being phase errors, while assuming that amplitude imbalances are absent. This assumption is made because quadrature image peaks are quite generally not observed in indirect dimensions when conventional HS [1,4] is employed on modern NMR spectrometers (this also implies that nuclear spin relaxation does not affect the two interferograms differently). Hence, amplitude imbalances can be neglected for CAM data acquisition and we focus on the phase errors. With identical amplitudes, one can readily derive a condition for $2\psi + \delta$ yielding maximal intensity of $A+$ (*i.e.*, $|\lambda^{A+}_{MHS}|$ being maximal):

$$\begin{aligned} &\frac{d\lambda^{A+}_{MHS}}{d(2\psi+\delta)} = \frac{d}{d(2\psi+\delta)}\left(\sin(2\psi+\delta+\Phi^{+}_{\psi}) + \sin(2\psi+\delta+\Phi^{-}_{\psi+\delta})\right) = 0 \\ &\Rightarrow 2\psi + \delta = (2n+1)\frac{\pi}{2} - \frac{\Phi^{+}_{\psi} + \Phi^{-}_{\psi+\delta}}{2} \quad n = 0, 1 \end{aligned} \quad (8)$$

For a signal with known phase errors Φ^{+}_{ψ} and $\Phi^{-}_{\psi+\delta}$, Eq. (8) allows one to adjust a primary phase shift to maximize intensity: for a given value of δ, ψ can be adjusted or *vice versa*. When considering multiple signals, adjustment of a primary phase shift depends on the *distribution of phase errors* and on their relative importance, *i.e.*, their weighting for the calculation of an averaged adjusted primary phase shift to maximize *overall* signal intensity. Importantly, the distribution of phase errors has to be measured only once for a given NMR experiment and instrumental set-up. This is because the adjusted primary phase can be used for other samples, as long as the r.f. pulse scheme of the NMR experiment and the set-up are not modified. If the phase errors of different signals have opposite signs, any adjustment leading to a signal gain for a one signal leads to a reduction of intensity for a signal associated with phase error of opposite sign. Eq. (8) thus reveals that without knowledge of the phase errors, the 'canonical' schemes defined by Eq. (6) are the best first choice.

6. Calculation of the time domain signal obtained with generalized canonical MHS.

With canonical primary phase shifts of $2\psi + \delta = \pi/2$ [Table 1(i)], Eq. (7) simplifies to

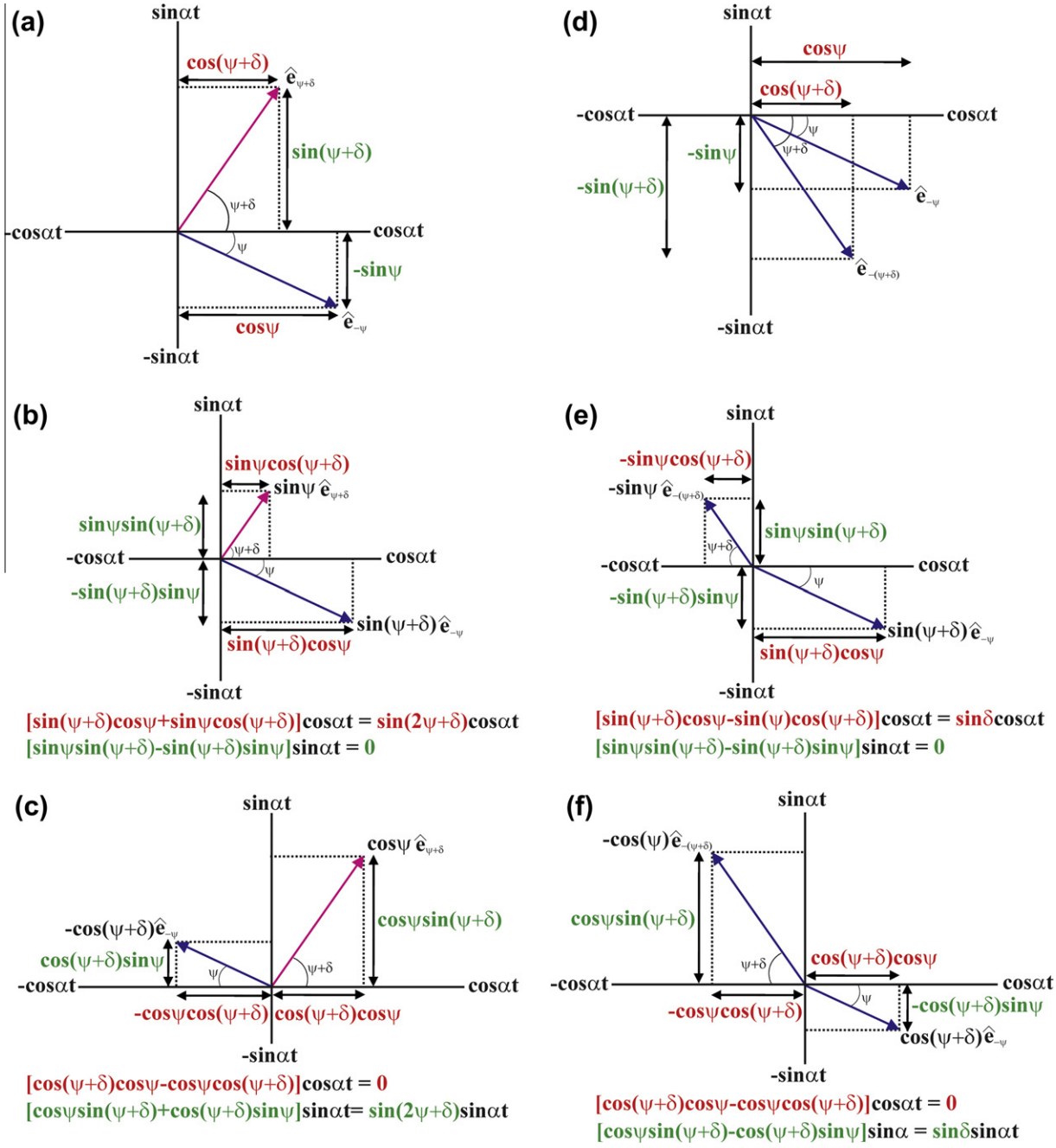

Fig. 1. Pictorial derivation of **D**-matrices for MHS (a–c) and forward HS (d–f). (a) The two interferograms leading to MHS quadrature detection are represented by unit vectors $\hat{e}_{-\psi}$ and $\hat{e}_{(\psi+\delta)}$ in a 2D plane spanned by the basis vectors cosαt and sinαt (with α being the chemical shift). The polar angles $-\psi$ and $(\psi + \delta)$ define the primary phase shifts and they are positive when measured anticlockwise. The projections of the unit vectors on the cosαt axis (cosine modulations) are shown in red while those on the sinαt axis (sine modulations) are shown in green. Forward sampling (blue unit vectors) leads to a negative polar angle resulting in, respectively, positive cosαt-axis and negative sinαt-axis projections, while backward sampling (magenta unit vectors) results in positive projections on both the cosαt- and the sinαt-axis (Eq. (7)). (b) Each of the two unit vectors is multiplied by the magnitude of the sinαt-axis projection of the other one, so that the sinαt-axis projections of the two resulting vectors cancel each other. This corresponds to the multiplication of the first row of the **D**-matrix with the interferogram vector (Eq. (4)). The cosαt-axis projections of the resulting vectors add up to give rise to a pure cosine modulation scaled by $\sin(2\psi + \delta)$, where $2\psi + \delta$ is the angle between the two unit vectors in (a). Inspection of the graph shows that the pure cosine modulated signal becomes maximal when $2\psi + \delta = \pi/2$ (Eq. (6)). (c) Each of the two unit vectors is multiplied by the magnitude of the cosαt-axis projection of the other one and the resulting vector in the direction of $\hat{e}_{-\psi}$ is then multiplied by -1, so that the cosαt-axis projections of the two resulting vectors cancel each other. This corresponds to the multiplication of the second row of the **D**-matrix with the interferogram vector (Eq. (4)). The sinαt-axis projections of the resulting vectors add up to give rise to a pure sine modulation, likewise scaled by $\sin(2\psi + \delta)$. Inspection of the graph shows that the sine modulated signal becomes maximal when $2\psi + \delta = \pi/2$ (Eq. (6)). (d) The two interferograms leading to forward HS quadrature detection are both forward sampled and are represented by unit vectors $\hat{e}_{-\psi}$ and $\hat{e}_{-(\psi+\delta)}$ with negative polar angles $-\psi$ and $-(\psi + \delta)$, respectively. (e) Each of the two unit vectors is multiplied by the magnitude of the sinαt-axis projection of the other one and the resulting vector in the direction of $\hat{e}_{-(\psi+\delta)}$ is then multiplied by -1, so that the sinαt-axis projections of the two resulting vectors cancel each other. This corresponds to the multiplication of the first row of the **D**-matrix with the interferogram vector [Eq. (S4)]. The cosαt-axis projections of the resulting vectors partially cancel each other to give rise to a pure cosine modulation scaled by sinδ, where δ is the angle between the two unit vectors in (d). Inspection of the graph shows that the pure cosine modulated signal becomes maximal when $\delta = \pi/2$ [Eq.(S60)]. (f) Each of the two unit vectors is multiplied by the magnitude of the cosαt-axis projection of the other one and the resulting vector in the direction of $\hat{e}_{-(\psi+\delta)}$ is then multiplied by -1, so that the cosαt-axis projections of the two resulting vectors cancel each other. This corresponds to the multiplication of the second row of the **D**-matrix with the interferogram vector [Eq. (S4)]. The sinαt-axis projections of the resulting vectors partially cancel each other to give rise to a pure sine modulation, likewise scaled by sinδ. Inspection of the graph shows that the sine modulated signal becomes maximal when $\delta = \pi/2$ [Eq. (S6)]. Notably, a 2D vector diagram related to HS was presented in [35] to exemplify 'CYCLOPS' phase cycling [1].

$$S_{\psi,\delta}(t) = \frac{1}{2}(I^{+}_{\psi}\cos\Phi^{+}_{\psi} + I^{-}_{\psi+\delta}\cos\Phi^{-}_{\psi+\delta})e^{i\alpha t} + \frac{1}{2}\left(I^{+}_{\psi}\sin\Phi^{+}_{\psi} - I^{-}_{\psi+\delta}\sin\Phi^{-}_{\psi+\delta}\right)e^{i\frac{\pi}{2}}e^{i\alpha t} + \frac{1}{2}(I^{+}_{\psi}\sin(\delta-\Phi^{+}_{\psi}) - I^{-}_{\psi+\delta}\sin(\delta+\Phi^{-}_{\psi+\delta}))e^{-i\alpha t} - \frac{1}{2}(I^{+}_{\psi}\cos(\delta-\Phi^{+}_{\psi}) - I^{-}_{\psi+\delta}\cos(\delta+\Phi^{-}_{\psi+\delta}))e^{i\frac{\pi}{2}}e^{-i\alpha t} \quad (9)$$

Inspection of Eq. (9) reveals that canonical sampling in the presence of secondary phase shifts and amplitude imbalances followed by generalized **D**-matrix transformation [Eq. (4)] yields *A*+ and *D*+ signal components which are independent of ψ and δ, while *A*− and *D*− depend on δ. Hence, δ can be adjusted so that quadrature signals are either largely absorptive or dispersive. As an illustration, Fig. 2 shows simulated MHS data for $\psi = \pi/4$ and $\delta = 0$. For Fig. 2a, the amplitudes and secondary phase shifts are set to $I^{+}_{\psi} = 0.8, I^{-}_{\psi} = 0.5, \Phi^{+}_{\psi} = -10^{0}, \Phi^{-}_{\psi} = 9^{0}$, and the resulting mixed phases of the two peaks at $\pm\alpha$ are apparent.

7. Transformation into frequency domain.

After **D**-matrix transformation, the two MHS interferograms result in complex time domain signals [Eq. (9)] as obtained directly with widely used HS (*i.e.*, without linear combination of interferograms). As a result, fundamental features of FT NMR spectroscopy are not affected, *e.g.* the implications of the causality principle [1] yielding the Hilbert transform relationship between real and imaginary part of the complex time domain signal [1]. Hence, transformation [30] into frequency domain and data processing in general [30] is accomplished in the same manner as for spectra acquired with HS, and generalized theory for MHS is presented here for the time domain. Moreover, **D**-matrix transformation yields *linear* combinations of time domain interferograms. In contrast to transformations into frequency domain, **D**-matrix transformation is thus not affected by the time domain data being discrete or continuous. Hence, effects arising from the discreteness of time domain data upon transformation into the frequency domain are the same as those which are well known for spectra acquired with HS [1,3]. It is, however, worth noting that FT of a complex signal obtained with discrete HS and delayed acquisition results in baseline distortion [31], unless the first order phase correction is 0° or 180°. Since CAM data acquisition eliminates all secondary phase shifts including those resulting from delayed acquisition (which should be avoided to maximize signal intensity; see introduction), the time domain spectra after **D**-matrix transformation correspond to conventional spectra acquired with 0° first order phase correction. As a result, spectra obtained with CAM data acquisition do not exhibit such baseline distortions.

2.2. Dual mirrored hypercomplex sampling (DMHS)

When employed for CAM data acquisition, DHMS aims at eliminating quadrature image peaks arising from phase errors [16]. With the generalized **D**-matrix of Eq. (4) and when increasing ψ by $\pi/2$ while δ remains the same when compared with the derivation of Eq. (7), the complex time domain signal is proportional to

$$S_{\psi+\frac{\pi}{2},\delta}(t) \propto -\frac{1}{2}\left(I^{+}_{\psi+\frac{\pi}{2}}\sin(2\psi+\delta+\Phi^{+}_{\psi+\frac{\pi}{2}}) + I^{-}_{\psi+\frac{\pi}{2}+\delta}\sin(2\psi+\delta+\Phi^{-}_{\psi+\frac{\pi}{2}+\delta})\right)e^{i\alpha t} + \frac{1}{2}\left(I^{+}_{\psi+\frac{\pi}{2}}\cos(2\psi+\delta+\Phi^{+}_{\psi+\frac{\pi}{2}}) - I^{-}_{\psi+\frac{\pi}{2}+\delta}\cos(2\psi+\delta+\Phi^{-}_{\psi+\frac{\pi}{2}+\delta})\right)e^{i\frac{\pi}{2}}e^{i\alpha t} + \frac{1}{2}\left(I^{+}_{\psi+\frac{\pi}{2}}\sin\left(\delta-\Phi^{+}_{\psi+\frac{\pi}{2}}\right) - I^{-}_{\psi+\frac{\pi}{2}+\delta}\sin(\delta+\Phi^{-}_{\psi+\frac{\pi}{2}+\delta})\right)e^{-i\alpha t} - \frac{1}{2}\left(I^{+}_{\psi+\frac{\pi}{2}}\cos(\delta-\Phi^{+}_{\psi+\frac{\pi}{2}}) - I^{-}_{\psi+\frac{\pi}{2}+\delta}\cos(\delta+\Phi^{-}_{\psi+\frac{\pi}{2}+\delta})\right)e^{i\frac{\pi}{2}}e^{-i\alpha t} \quad (10)$$

As an illustration, Fig. 2b shows simulated MHS data for $\psi = 3\pi/4$ and $\delta = 0$. Here, the amplitudes and secondary phase shifts are set to $I^{+}_{\psi+\delta} = 0.9, I^{-}_{\psi+\delta} = 0.55, \Phi^{+}_{\psi+\delta} = 12^{\circ}$, and $\Phi^{-}_{\psi+\delta} = -5^{\circ}$ and the resulting mixed phases and of the two peaks located at $\pm\alpha$ are apparent.Subtraction of $S_{\psi+\frac{\pi}{2},\delta}(t)$ in Eq. (10) from $S_{\psi,\delta}(t)$ in Eq. (7) then yields the complex time domain signal for DMHS, which is proportional to

$$\begin{aligned} S_{\psi,\delta}(t) - S_{\psi+\frac{\pi}{2},\delta}(t) \propto{}& \frac{1}{2}(I^{+}_{\psi}\sin(2\psi+\delta+\Phi^{+}_{\psi}) + I^{-}_{\psi+\delta}\sin(2\psi+\delta+\Phi^{-}_{\psi+\delta}) \\ &+ I^{+}_{\psi+\frac{\pi}{2}}\sin(2\psi+\delta+\Phi^{+}_{\psi+\frac{\pi}{2}}) + I^{-}_{\psi+\frac{\pi}{2}+\delta}\sin(2\psi+\delta+\Phi^{-}_{\psi+\frac{\pi}{2}+\delta}))e^{i\alpha t} \\ &- \frac{1}{2}(I^{+}_{\psi}\cos(2\psi+\delta+\Phi^{+}_{\psi}) - I^{-}_{\psi+\delta}\cos(2\psi+\delta+\Phi^{-}_{\psi+\delta}) \\ &+ I^{+}_{\psi+\frac{\pi}{2}}\cos(2\psi+\delta+\Phi^{+}_{\psi+\frac{\pi}{2}}) - I^{-}_{\psi+\frac{\pi}{2}+\delta}\cos(2\psi+\delta+\Phi^{-}_{\psi+\frac{\pi}{2}+\delta}))e^{i\frac{\pi}{2}}e^{i\alpha t} \\ &+ \frac{1}{2}(I^{+}_{\psi}\sin(\delta-\Phi^{+}_{\psi}) - I^{-}_{\psi+\delta}\sin(\delta+\Phi^{-}_{\psi+\delta}) - I^{+}_{\psi+\frac{\pi}{2}}\sin(\delta-\Phi^{+}_{\psi+\frac{\pi}{2}}) \\ &+ I^{-}_{\psi+\frac{\pi}{2}+\delta}\sin(\delta+\Phi^{-}_{\psi+\frac{\pi}{2}+\delta}))e^{-i\alpha t} - \frac{1}{2}(I^{+}_{\psi}\cos(\delta-\Phi^{+}_{\psi}) \\ &- I^{-}_{\psi+\delta}\cos(\delta+\Phi^{-}_{\psi+\delta}) - I^{+}_{\psi+\frac{\pi}{2}}\cos(\delta-\Phi^{+}_{\psi+\frac{\pi}{2}}) \\ &+ I^{-}_{\psi+\frac{\pi}{2}+\delta}\cos(\delta+\Phi^{-}_{\psi+\frac{\pi}{2}+\delta}))e^{i\frac{\pi}{2}}e^{-i\alpha t} \\ ={}& \lambda^{A+}_{DMHS}e^{i\alpha t} + \lambda^{D+}_{DMHS}e^{i\frac{\pi}{2}}e^{i\alpha t} + \lambda^{A-}_{DMHS}e^{-i\alpha t} + \lambda^{D-}_{DMHS}e^{i\frac{\pi}{2}}e^{-i\alpha t} \end{aligned} \quad (11)$$

(Note that the second data set can also be recorded by increasing ψ by $\pi/2$ and δ by π. Then, $S_{\psi+\frac{\pi}{2},\delta}(t)$ and $S_{\psi,\delta}(t)$ need to be added.) Inspection of Eq. (11) reveals that for non-identical amplitudes and/or phase errors, the dispersive components are only partially eliminated [Fig. 2c–e]. In the limit of $I^{+}_{\psi} = I^{-}_{\psi+\delta} = I^{+}_{\psi+\frac{\pi}{2}} = I^{-}_{\psi+\frac{\pi}{2}+\delta} =$ I and $\Phi^{+}_{\psi} = \Phi^{-}_{\psi+\delta} = \Phi^{+}_{\psi+\frac{\pi}{2}} = \Phi^{-}_{\psi+\frac{\pi}{2}+\delta} = \Phi$,

Eq. (11) simplifies to

$$S_{\psi,\delta}(t) - S_{\psi+\frac{\pi}{2},\delta}(t) \propto 2I\sin(2\psi+\delta+\Phi)e^{i\alpha t} \quad (12)$$

Inspection of Eq. (12) shows (i) that for arbitrary primary phases one can obtain CAM spectra which are devoid of both dispersive peak components and quadrature image peaks [Fig. 2(f)], and (ii) that signal intensity is maximal when the condition of Eq. (6) is fulfilled. Analogous theory for HS, as well as for its extension to novel DHS [16], is presented in Section II of the Supplementary Material.

2.3. Figures of merit (FOM)

Inspection of the equations for the complex time domain signals obtained with MHS [Eq. (7)], DMHS [Eq. (11)], HS [Eq. (S7)] and DHS [Eq. (S10)] shows that the canonical sampling schemes (Table 1) perform differently for CAM NMR data acquisition when secondary phase shifts being phase errors depend on sampling directionality and/or primary phase shifts (or when imbalances of amplitudes are encountered). Comparison is, however, impeded by the intricate dependence of the relative intensities (*i.e.*, λ-coefficients) on secondary phase shifts and amplitude imbalances. Since the elimination of (i) dispersive signal components located at $+\alpha$ in the frequency domain and (ii) quadrature signals located at $-\alpha$ in the frequency domain are the two aims of CAM data acquisition, we define two corresponding figures of merit (FOM), M^{D} and M^{Q}, in order to benchmark the performance of the schemes. These FOMs are defined as

$$M^{D} = \frac{|\lambda^{A+}|}{|\lambda^{A+}| + |\lambda^{D+}|} \quad (13)$$

and

$$M^{Q} = M^{D} = \frac{|\lambda^{A+}| + |\lambda^{D+}|}{|\lambda^{A+}| + |\lambda^{D+}| + |\lambda^{A-}| + |\lambda^{D-}|} \quad (14)$$

which are equal to 1 for complete elimination of dispersive components and quadrature signals, respectively.

2.4. Calculation of time domain amplitudes and secondary phase shifts from frequency domain signals for canonical MHS

Accurate measurement of time domain amplitudes and secondary phase shifts is required to (i) assess the performance of a given sampling scheme for CAM data acquisition and to (ii) analyze NMR experiments in which parameters are encoded in amplitude imbalances or secondary phase shifts. Quite generally, the time domain signal results from the superposition of a large number of individual signals, so that secondary phase shifts and amplitudes are preferably calculated from phases and intensities registered for well resolved frequency domain peaks. To ensure accurate mapping of time domain phase shifts and amplitudes onto frequency domain phases and amplitudes, such analysis needs to rely on a *unitary* transformation into the frequency domain (*e.g.*, FT employed *without* prior linear prediction [3,30] of time domain data) followed by measurement of intensities and phases of frequency domain peaks.

Here we present equations relating time and frequency domain parameters resulting from FT of time domain data sampled with the canonical schemes of Table 1. In the following, $\tilde{I}_{+\alpha}$ and $\theta_{+\alpha}$ shall denote, respectively, intensity and phase of a frequency domain peak located at $+\alpha$, and, correspondingly, $\tilde{I}_{-\alpha}$ and $\theta_{-\alpha}$ denote intensity and phase of the quadrature image peak at $-\alpha$.

With Eq. (6), $\tilde{I}_{+\alpha}, \tilde{I}_{-\alpha}, \theta_{+\alpha}$ and $\theta_{-\alpha}$ are given by (see Section III.1 of the Supplementary Material for intermediate steps of calculations):

$$\begin{aligned}
\tilde{I}_{+\alpha} &= \frac{1}{2}\sqrt{I_{\psi}^2 + I_{\psi+\delta}^2 - 2I_{\psi}I_{\psi+\delta}\cos(2(2\psi+\delta)+\Phi_{\psi}+\Phi_{\psi+\delta})} \\
\tilde{I}_{-\alpha} &= \frac{1}{2}\sqrt{I_{\psi}^2 + I_{\psi+\delta}^2 - 2I_{\psi}I_{\psi+\delta}\cos(\Phi_{\psi}+\Phi_{\psi+\delta})} \\
\tan\theta_{+\alpha} &= -\frac{I_{\psi}\cos(2\psi+\delta+\Phi_{\psi}) - I_{\psi+\delta}\cos(2\psi+\delta+\Phi_{\psi+\delta})}{I_{\psi}\sin(2\psi+\delta+\Phi_{\psi}) + I_{\psi+\delta}\sin(2\psi+\delta+\Phi_{\psi+\delta})} \\
\tan\theta_{-\alpha} &= -\frac{I_{\psi}\cos(\delta-\Phi_{\psi}) - I_{\psi+\delta}\cos(\delta+\Phi_{\psi+\delta})}{I_{\psi}\sin(\delta-\Phi_{\psi}) - I_{\psi+\delta}\sin(\delta+\Phi_{\psi+\delta})}
\end{aligned} \tag{15}$$

so that

$$\begin{aligned}
I_{\psi} &= \sqrt{\tilde{I}_{+\alpha}^2+\tilde{I}_{-\alpha}^2-2\tilde{I}_{+\alpha}\tilde{I}_{-\alpha}\sin(\theta_{+\alpha}+\theta_{-\alpha}-\delta)} \text{ for } 2\psi+\delta=\pi/2\ (n=0) \\
I_{\psi} &= \sqrt{\tilde{I}_{+\alpha}^2+\tilde{I}_{-\alpha}^2+2\tilde{I}_{+\alpha}\tilde{I}_{-\alpha}\sin(\theta_{+\alpha}+\theta_{-\alpha}-\delta)} \text{ for } 2\psi+\delta=3\pi/2\ (n=1) \\
I_{\psi+\delta} &= \sqrt{\tilde{I}_{+\alpha}^2+\tilde{I}_{-\alpha}^2+2\tilde{I}_{+\alpha}\tilde{I}_{-\alpha}\sin(\theta_{+\alpha}+\theta_{-\alpha}-\delta)} \text{ for } 2\psi+\delta=\pi/2\ (n=0) \\
I_{\psi+\delta} &= \sqrt{\tilde{I}_{+\alpha}^2+\tilde{I}_{-\alpha}^2-2\tilde{I}_{+\alpha}\tilde{I}_{-\alpha}\sin(\theta_{+\alpha}+\theta_{-\alpha}-\delta)} \text{ for } 2\psi+\delta=3\pi/2\ (n=1) \\
\tan\Phi_{\psi} &= \frac{\tilde{I}_{+\alpha}\sin\theta_{+\alpha}-\tilde{I}_{-\alpha}\cos(\theta_{-\alpha}-\delta)}{\tilde{I}_{+\alpha}\cos\theta_{+\alpha}-\tilde{I}_{-\alpha}\sin(\theta_{-\alpha}-\delta)} \text{ for } 2\psi+\delta=\pi/2\ (n=0) \\
\tan\Phi_{\psi} &= \frac{\tilde{I}_{+\alpha}\sin\theta_{+\alpha}+\tilde{I}_{-\alpha}\cos(\theta_{-\alpha}-\delta)}{\tilde{I}_{+\alpha}\cos\theta_{+\alpha}+\tilde{I}_{-\alpha}\sin(\theta_{-\alpha}-\delta)} \text{ for } 2\psi+\delta=3\pi/2\ (n=1) \\
\tan\Phi_{\psi+\delta} &= -\frac{\tilde{I}_{+\alpha}\sin\theta_{+\alpha}+\tilde{I}_{-\alpha}\cos(\theta_{-\alpha}-\delta)}{\tilde{I}_{+\alpha}\cos\theta_{+\alpha}+\tilde{I}_{-\alpha}\sin(\theta_{-\alpha}-\delta)} \text{ for } 2\psi+\delta=\pi/2\ (n=0) \\
\tan\Phi_{\psi+\delta} &= -\frac{\tilde{I}_{+\alpha}\sin\theta_{+\alpha}-\tilde{I}_{-\alpha}\cos(\theta_{-\alpha}-\delta)}{\tilde{I}_{+\alpha}\cos\theta_{+\alpha}-\tilde{I}_{-\alpha}\sin(\theta_{-\alpha}-\delta)} \text{ for } 2\psi+\delta=3\pi/2\ (n=1)
\end{aligned} \tag{16}$$

Analogous equations for HS are presented for HS in Sections III.2 and III.3 of the Supplementary Material.

3. Results and discussion

3.1. Measurement of amplitudes and secondary phase shifts

The generalized theory of mirrored NMR time domain sampling enables one to confirm for a given NMR experiment if assumptions are accurate which were previously made for implementation and employment of CAM data acquisition [16], *i.e.*, having time domain signal amplitudes and phase errors that are independent of time domain sampling direction and primary phase shifts. Although visual inspection of spectra recorded with CAM data acquisition showed that phase errors are eliminated rather efficiently (see Figs. 2–4 in [16]), it remained an open question if accurate measurement of frequency domain phases and amplitudes followed by calculation of time domain secondary phase shifts and amplitudes reveals minor, but significant deviations from the above stated assumptions.

As an example, we analyze here signals in simultaneous constant time 2D [$^{13}C^{aliphatic}/^{13}C^{aromatic}$, ^{1}H]-HSQC spectra that were recorded [16] with different canonical schemes (Table 1) for the ^{13}C, ^{15}N-labeled 8 kDa structural genomics target protein CaR178. When employing HS [4] without delayed acquisition, a small first order phase correction is required due to off-resonance effects of ^{13}C r.f. pulses. Such a correction can ensure that virtually absorptive peaks are registered for the aliphatic ^{13}C–^{1}H moieties, while the peaks arising from aromatic moieties, which are folded along ω_1 (^{13}C), exhibit residual dispersive components [Fig. 3a]. These cannot be eliminated by a first-order phase correction since such a correction would then re-introduce dispersive components for the aliphatic peaks. MHS enables one to transfer the dispersive peak components into quadrature image peaks [Fig. 3b] and those can be eliminated by use of DHMS [Fig. 3c].

With Eqs. (16), (S28) and (S37), the time domain amplitudes and secondary phase shifts of the two interferograms recorded for a given acquisition scheme were calculated from frequency domain intensities and phases for three well resolved aromatic signals and their corresponding quadrature signals [Fig. 3(b), Table 2]. The errors of the time domain parameters were calculated from the experimental errors of the measured frequency domain parameters using laws of error propagation (see Eqs. S98 in Section VII.1 and S102 in Section VII.2 of the Supplementary Material). Comparison of time domain amplitudes and secondary phase shifts for the interferograms acquired for MHS with $\psi = \pi/4$, $\delta = 0$ and $\psi = 3\pi/4$, $\delta = 0$ [Table 2(i)], and forward and backward sampled HS [Table 2(ii)] shows that these parameters are, within the experimental errors, indeed independent of time domain sampling direction and primary phase shifts. This is in agreement with the fact that dispersive components and corresponding quadrature image peaks are completely eliminated when employing DMHS [Fig. 3c].

The absence of any significant time domain amplitude imbalances is expected since the setting of r.f. pulse phases and widths, as well as signal detection are highly accurate and reproducible on modern spectrometers. This is in agreement with the fact that quadrature image peaks in indirect dimensions of multidimensional spectra are quite generally not detected. The finding that phase errors are also independent of sampling direction and primary phase shifts is, *a priori*, a finding specific for the experiment analyzed here, *i.e.*, for simultaneous constant time 2D [$^{13}C^{aliphatic}/^{13}C^{aromatic}$, ^{1}H]-HSQC recorded for proteins. However, such 2D [^{13}C, ^{1}H]-HSQC [3] consists of two INEPT-type [1] steps which themselves represent modules widely used for the design of heteronuclear NMR experiments relying on through-bond polarization transfer [3]. Hence, this finding indicates that CAM data acquisition [16] can be employed for such experiments, unless distinct features of their design give rise to phase shifts being dependent on primary phase or sampling directionality.

3.2. Comparison of canonical MHS/HS schemes for CAM data acquisition

The generalized theory of time domain sampling presented here enables one to compare the performance of the canonical sampling

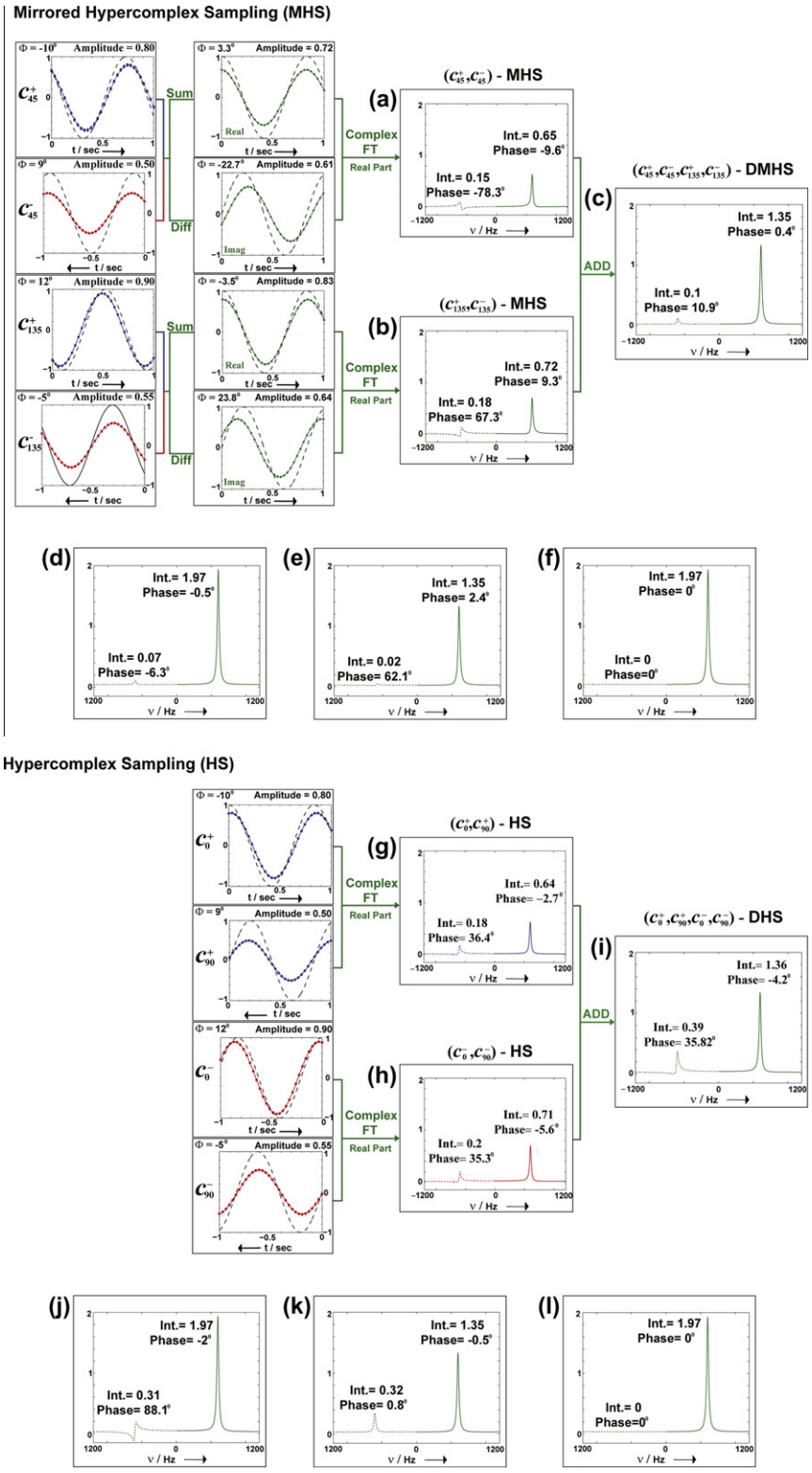

Fig. 2. Simulated spectral data for MHS (a–f) and HS (g–l) NMR data acquisition obtained for non-identical amplitude and secondary phase shift. Forward and backward time domain sampled interferograms are shown, respectively, in blue and red, and linear combinations of time or frequency domain data are depicted in green. For comparison, the dashed gray lines represent time domain data of unit amplitude and $\Phi = 0°$. The amplitudes and the secondary phase shifts for each interferogram are given, respectively, at the top right and left corners of each box. Intensities and phases of each frequency domain peak are also provided. The intensities and phases of the frequency domain spectra were calculated using Eq. (15) for MHS, Eqs. (S29) and (S30) of the Supplementary Material for forward HS and Eqs. (S38) and (S39) of the Supplementary Material for backward HS. Amplitude and secondary phase imbalances result in peaks with mixed phases located at $+\alpha = +600$ Hz (solid line) and the corresponding quadrature image peak position at $-\alpha = -600$ Hz (dashed line) for both MHS (a, b) and HS (g, h). With non-identical amplitudes and secondary phase shifts, DMHS (c) and DHS (i) eliminate dispersive and quadrature image peak components only partially. (d, j) Frequency domain signals obtained for MHS and HS with different secondary phase shifts for the two interferograms but identical amplitudes, showing that elimination of dispersive peak components is incomplete. (e, k) MHS and HS with different amplitudes for the two interferograms but identical secondary phase shifts of 10°, showing that elimination of dispersive peak components is incomplete. (f, l) MHS and HS with identical amplitude and secondary phase shifts for all interferograms resulting in complete elimination of dispersive peak components as described previously [16].

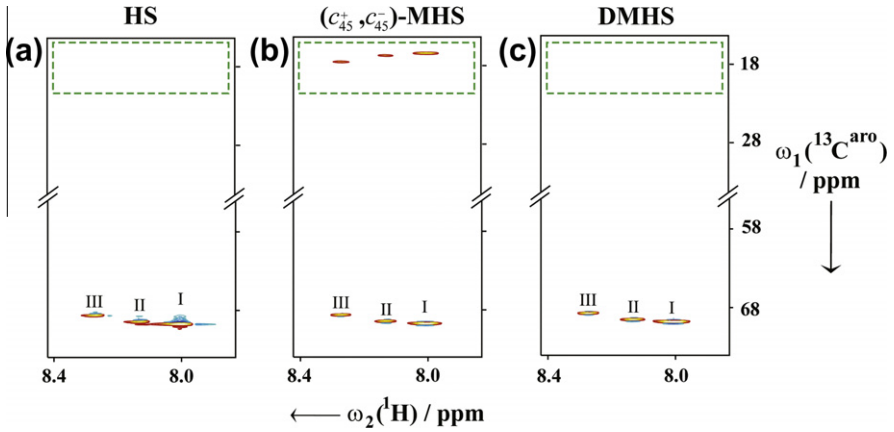

Fig. 3. Contour plots from simultaneous constant time 2D [$^{13}C^{aliphatic}/^{13}C^{aromatic}$]-HSQC spectra. Plots comprising three aromatic signals (denoted as I, II and III; see also Table 2) and their corresponding quadrature image peaks (shown within dashed green boxes) taken from spectra acquired with (a) forward HS, (b) (c^{+}_{45}, c^{-}_{45})-MHS and (c) $(c^{+}_{45}, c^{-}_{45}, c^{+}_{\bar{1}35}, c^{-}_{\bar{1}35})$-DMHS. In (a), dispersive peak components are apparent, which are 'moved' into absorptive quadrature image peaks in (b). In (c), dispersive peak components and quadrature image peaks are eliminated.

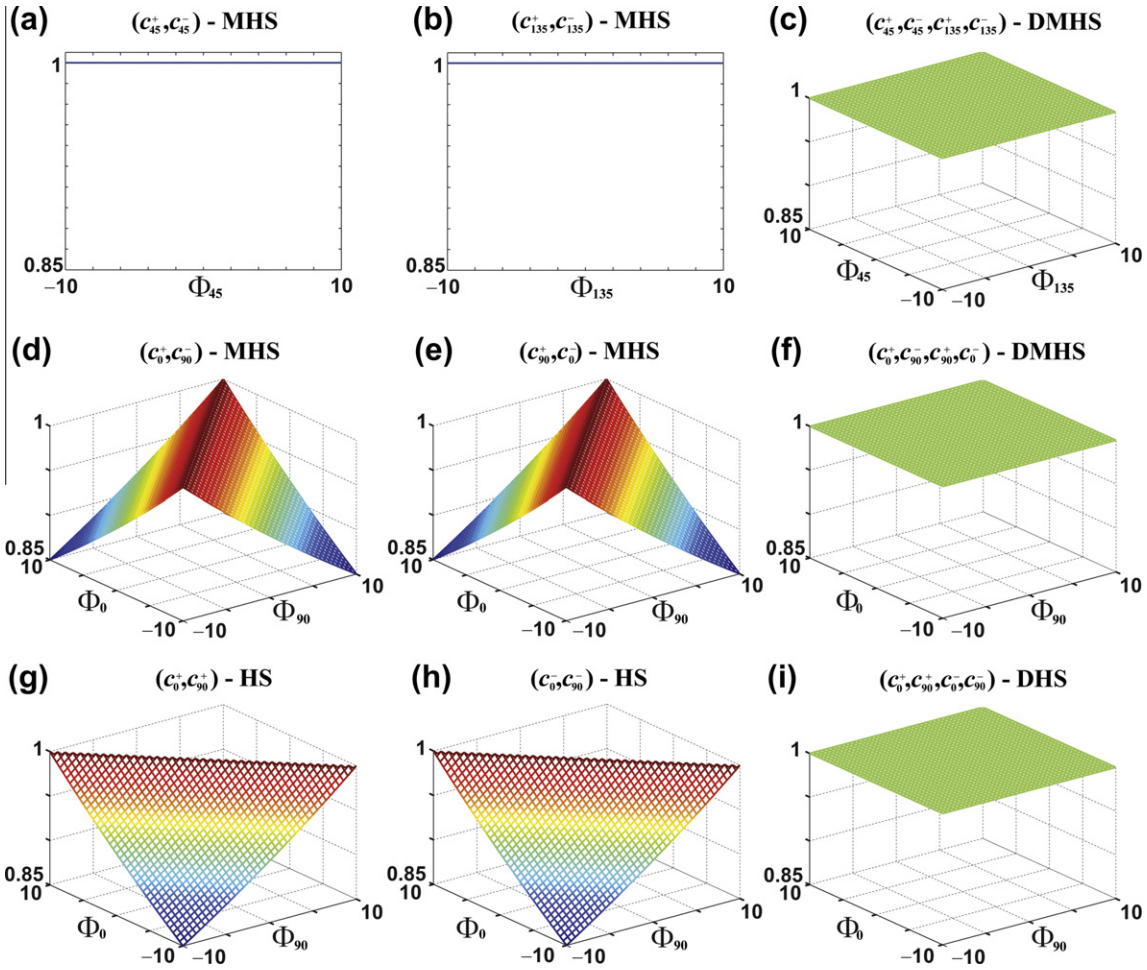

Fig. 4. Plots of figures of merit for elimination of dispersive peak components. M^D was calculated according to Eq. (13) when phase errors ('secondary phase shifts') depend on primary phase shifts but *not* on the sampling directionality, that is, $\Phi^{+}_{\psi} = \Phi^{-}_{\psi} = \Phi_{\psi}$ and $\Phi^{+}_{\psi+\delta} = \Phi^{-}_{\psi+\delta} = \Phi_{\psi+\delta}$. The FOM is calculated for a range of ±10°. (a) (c^{+}_{45}, c^{-}_{45})-MHS, (b) $(c^{+}_{\bar{1}35}, c^{-}_{\bar{1}35})$-MHS, (c) $(c^{+}_{45}, c^{-}_{45}, c^{+}_{\bar{1}35}, c^{-}_{\bar{1}35})$-DMHS, (d) (c^{+}_{0}, c^{-}_{90})-MHS, (e) (c^{+}_{90}, c^{-}_{0})-MHS, (f) $(c^{+}_{0}, c^{-}_{90}, c^{+}_{90}, c^{-}_{0})$-DMHS, (g) forward HS, (h) backward HS, and (i) DHS. Note that (c^{+}_{45}, c^{-}_{45})-MHS and $(c^{+}_{\bar{1}35}, c^{-}_{\bar{1}35})$-MHS are functions of only one phase error (a,b). (c^{+}_{45}, c^{-}_{45})-MHS and $(c^{+}_{\bar{1}35}, c^{-}_{\bar{1}35})$-MHS, and dual MHS or HS give rise to ideal CAM data acquisition ($M^D = 1$).

schemes [Table 1] for CAM data acquisition [16] when phase errors depend moderately (*e.g.*, up to ±10°) on primary phase shifts or sampling directionality. For future routine applications, it is of particular interest to assess the *robustness* of alternative canonical CAM data acquisition schemes with respect to such variations of phase errors, *i.e.*, the degree to which dispersive peak components

Table 2
Analysis of 2D [$^{13}C^{aliphatic}/^{13}C^{aromatic}$, ^{1}H]-HSQC spectra.

	$\psi = 45°$ ($\delta = 0°$)			$\psi = 135°$ ($\delta = 0°$)			Dual		
	Peak I	Peak II	Peak III	Peak I	Peak II	Peak III	Peak I	Peak II	Peak III
(i) Mirrored hypercomplex sampling (MHS)[a]									
$\tilde{I}_{+\alpha}(\times 10^5)$	−4.27 ± 0.02	−1.48 ± 0.02	−1.58 ± 0.02	−4.29 ± 0.02	−1.5 ± 0.02	−1.62 ± 0.02	−8.53 ± 0.02	−2.96 ± 0.02	−3.22 ± 0.02
$\theta_{+\alpha}$	1.0 ± 0.5°	0.3 ± 1.5°	−2.6 ± 1.3°	0.35 ± 0.5°	0.2 ± 1.5°	0.0 ± 1.3°	0.7 ± 0.4°	0.3 ± 1.0°	−1.3 ± 1.0°
$\tilde{I}_{-\alpha}(\times 10^5)$	1.29 ± 0.02	0.41 ± 0.02	0.45 ± 0.02	−1.25 ± 0.02	−0.46 ± 0.02	−0.46 ± 0.02	0	0	0
$\theta_{-\alpha}$	0.5 ± 1.7°	−1.9 ± 4.8°	−10.5 ± 4.8°	0.5 ± 1.7°	5.8 ± 5.4°	−7.5 ± 4.6°	0	0	0
$I^{+}_{\psi}(\times 10^5)$	4.49 ± 0.04	1.52 ± 0.04	1.54 ± 0.04	4.49 ± 0.04	1.61 ± 0.05	1.62 ± 0.04	NA	NA	NA
Φ^{+}_{ψ}	17.7 ± 0.5°	16.0 ± 1.6°	13.8 ± 1.4°	16.5 ± 0.5°	16.8 ± 1.6°	16.1 ± 1.4°	NA	NA	NA
$I^{-}_{\psi}(\times 10^5)$	4.43 ± 0.04	1.55 ± 0.04	1.74 ± 0.04	4.45 ± 0.04	1.52 ± 0.05	1.74 ± 0.04	NA	NA	NA
Φ^{-}_{ψ}	16.0 ± 0.5°	15.2 ± 1.6°	17.1 ± 1.5°	16.0 ± 0.5°	17.4 ± 1.6°	15.1 ± 1.4°	NA	NA	NA
(ii) Hypercomplex sampling (HS)[a]									
	Forward sampling			Backward sampling			Dual sampling		
	Peak I	Peak II	Peak III	Peak I	Peak II	Peak III	Peak I	Peak II	Peak III
$\tilde{I}_{+\alpha}(\times 10^5)$	−2.93 ± 0.01	−0.97 ± 0.01	−1.07 ± 0.01	−2.85 ± 0.01	−1.0 ± 0.01	−1.08 ± 0.01	−5.71 ± 0.02	−1.96 ± 0.02	−2.13 ± 0.02
$\theta_{+\alpha}$	−15.6 ± 0.5°	−12.3 ± 1.5°	−15.6 ± 1.4°	16.7 ± 0.5°	16.3 ± 1.5°	14.2 ± 1.4°	0.6 ± 0.4°	2.0 ± 1.1°	−0.6 ± 1.0°
$\tilde{I}_{-\alpha}(\times 10^5)$	0	0	0	0	0	0	0	0	0
$\theta_{-\alpha}$	0	0	0	0	0	0	0	0	0
$I_{\psi}(\times 10^5)$	2.93 ± 0.01	0.97 ± 0.01	1.07 ± 0.01	2.85 ± 0.01	1.0 ± 0.01	1.08 ± 0.01	NA	NA	NA
Φ_{ψ}	15.6 ± 0.5°	12.3 ± 1.5°	15.6 ± 1.4°	16.7 ± 0.5°	16.3 ± 1.5°	14.2 ± 1.4°	NA	NA	NA
$I_{\psi+\delta}(\times 10^5)$	2.93 ± 0.01	0.97 ± 0.01	1.07 ± 0.01	2.85 ± 0.01	1.0 ± 0.01	1.08 ± 0.01	NA	NA	NA
$\Phi_{\psi+\delta}$	15.6 ± 0.5°	12.3 ± 1.5°	15.6 ± 1.4°	16.7 ± 0.5°	16.3 ± 1.5°	14.2 ± 1.4°	NA	NA	NA

[a] See Section VII of the Supplementary Material for the estimation of errors.

and quadrature image peaks are eliminated in spite of the dependency.

Specifically, the impact of variations of secondary phase shifts can be quantitatively compared using the FOMs M^D for elimination of the dispersive peak component located at frequency $+\alpha$ [Eq. (13)] and M^Q for elimination of the quadrature image peak located at frequency $-\alpha$ [Eq. (14)]. Ideally, $M^D = M^Q = 1$ for CAM data acquisition which implies their complete elimination. Here we discuss separately the cases where an inequality of secondary phase shifts [Eq. (1)] originates from a change of primary phase shift, or from a change in sampling direction.

First, we address the case that the phase errors depend on the primary phase shifts but are *independent* of the directionality of time domain sampling. Comparison of M^D [Fig. 4] shows that (c^{+}_{45}, c^{-}_{45})-MHS is the preferred choice if the elimination of the dispersive component is of highest priority. For this scheme, elimination is complete ($M^D = 1$) since the primary phase shift is the same for the two interferograms used to construct the complex time domain signal, that is, data acquisition is insensitive to any variation of the phase error with varying primary phase shift. When using HS, dual sampling must be employed to achieve $M^D = 1$. If the elimination of the quadrature image peaks is of comparable importance, $(c^{+}_{0}, c^{-}_{90}, c^{+}_{90}, c^{-}_{0})$-DMHS and DHS (Fig. 5f and i) are preferred. Remarkably, M^Q drops by only ~1% for phase error differences between −10° and 10°, while a drop of ~15% is registered for $(c^{+}_{45}, c^{-}_{45}, c^{+}_{135}, c^{-}_{135})$-DMHS [Fig. 5c]. Thus, in applications where quadrature image peaks are in the noise or appear in otherwise empty spectral regions, (c^{+}_{45}, c^{-}_{45})-MHS and $(c^{+}_{135}, c^{-}_{135})$-MHS are recommended, while in applications where it is mandatory that quadrature image peaks are eliminated $(c^{+}_{0}, c^{-}_{90}, c^{+}_{90}, c^{-}_{0})$-DMHS or DHS should be employed.

Second, we address the case that the phase errors depend on the directionality of time domain sampling but are *independent* of the primary phase shifts. Comparison of the values of M^D [Fig. S3 of the Supplementary Material] reveals the same drop of ~15% for phase error differences between −10° and 10°. This is due to the fact that all sampling schemes eliminate dispersive components by combining interferograms sampled in opposite directionality. Therefore, any dependence of phase errors on the sampling direction necessarily results in incomplete elimination of dispersive components. If the elimination of the quadrature image peaks is of comparable importance, HS is the preferred choice because no quadrature image peaks are generated ($M^Q = 1$) [see Fig. S4(g and h) of Supplementary Material].

Clearly, the above presented preferences for sampling schemes in case moderate variations of phase errors are encountered are relevant only when the S/N ratios of the signals are large enough to result in significant performance differences impacting spectral analysis. In Section VII.3 of the Supplementary Material, standard deviations of FOMs are calculated as a function of the S/N ratio, demonstrating that for phase error differences in the range of ±10°, performance differences become significant already for S/N ratios above ~5. Hence, the selection of the best suited sampling scheme is relevant even when data acquisition approaches the sensitivity limited data collection regime [32].

In view of the potential application of the different sampling schemes (Table 1), it is important to point at types of NMR experiments in which phase errors cannot be avoided entirely by optimization of r.f. pulse sequence design. For example, even an idealized description [1] of 'in-phase' magnetization transfer of total correlation spectroscopy [1,3] (TOCSY) using 'spin-modes' shows [1] that phase errors inevitably occur, and that they depend in a complex manner on spin–spin scalar coupling topology and mixing time [3]. Even though additional r.f. pulses (such as spin-lock purge pulses [3]) can reduce phase errors, their (nearly) complete elimination is quite challenging. In particular, this feature makes TOCSY sensitive to spectrometer imperfections so that a dependency of phase errors on primary phase shifts and sampling directionality often remains. Other types of spectroscopy which may well profit from the new sampling schemes include solid state NMR [1], which relies primarily on r.f. phase cycling to remove artifacts, spatially resolved NMR [33], in which phase errors arise from the required spatial selection, and pulse electron paramagnetic resonance (EPR) spectroscopy, which also relies on quadrature detection in the indirect dimension for multidimensional experiments (see, for example, Chapter 5 in [34]).

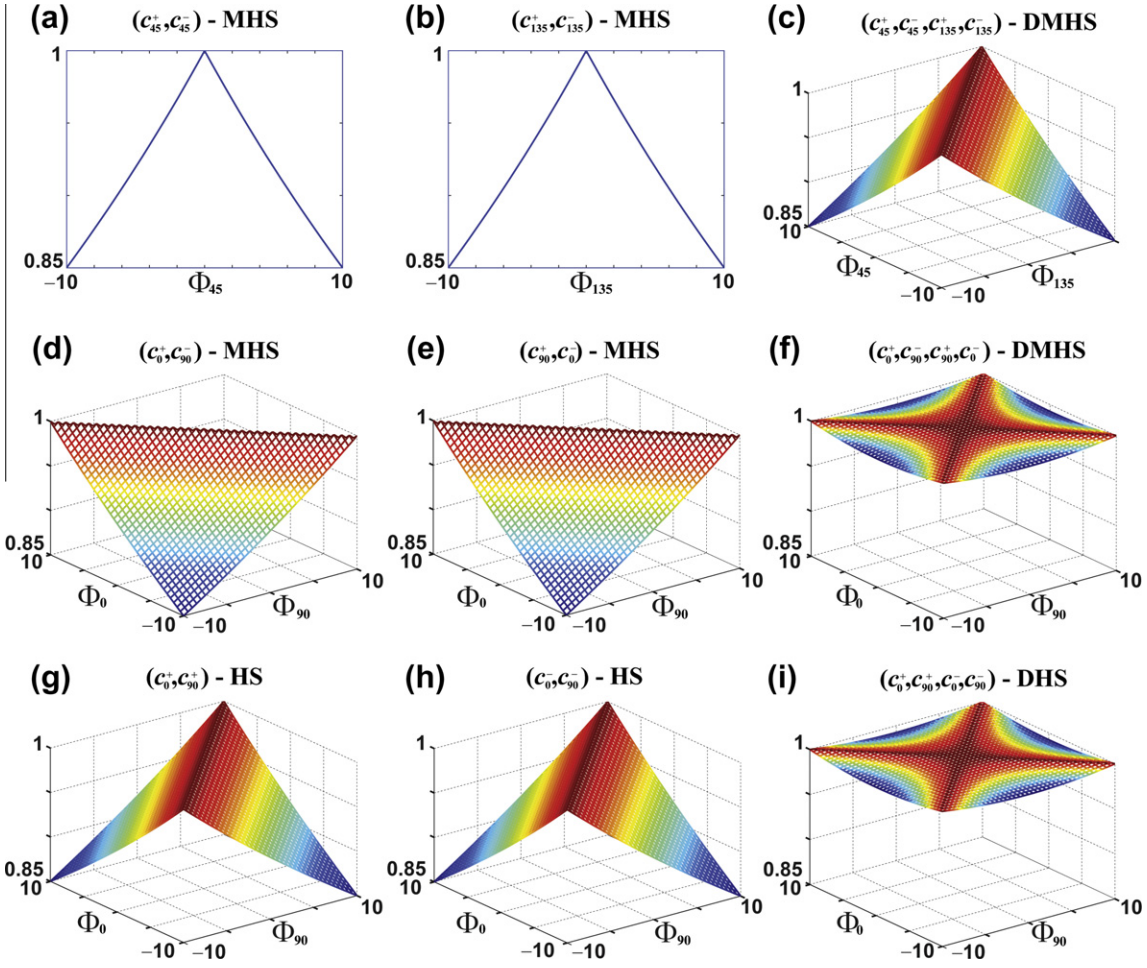

Fig. 5. Plots of figures of merit for elimination of quadrature image peak. M^{Q} was calculated using Eq. (14) when phase errors ('secondary phase shifts') depend on primary phase shifts but *not* on the sampling directionality, that is, $\Phi_{\psi}^{+}=\Phi_{\psi}^{-}=\Phi_{\psi}$ and $\Phi_{\psi+\delta}^{+}=\Phi_{\psi+\delta}^{-}=\Phi_{\psi+\delta}$. The FOM is calculated for a range of ±10°. (a) (c_{45}^{+},c_{45}^{-})-MHS, (b) $(c_{135}^{+},c_{135}^{-})$-MHS, (c) $(c_{45}^{+},c_{45}^{-},c_{135}^{+},c_{135}^{-})$-DMHS, (d) (c_{0}^{+},c_{90}^{-})-MHS, (e) (c_{90}^{+},c_{0}^{-})-MHS, (f) $(c_{0}^{+},c_{90}^{-},c_{90}^{+},c_{0}^{-})$-DMHS, (g) forward HS, (h) backward HS, and (i) and DHS Note that (c_{45}^{+},c_{45}^{-})-MHS and $(c_{135}^{+},c_{135}^{-})$-MHS are functions of only a single phase error (a, b).

4. Conclusions

The high accuracy and reproducibility of r.f. pulse phase setting and signal detection on modern NMR spectrometers ensures that CAM data acquisition can be readily employed for NMR experiments relying on through-bond polarization transfer, as long as they are designed such that *no* dependency of phase errors on primary phase shifts or sampling directionality is present. For experiments where this cannot be entirely accomplished, the comparison of the robustness of different schemes with respect to a moderate dependency of phase errors enables one to choose the one best suited for CAM data acquisition. Importantly, generally applicable techniques are not available for processing data acquired with HS [4] such that 'pseudo-random' phase errors are eliminated. This is because phase errors *not* correlated with frequency would require different 'local' phase corrections for each signal, which is not feasible when signals overlap.

Using the previously described tensor product description to employ HMS for multiple indirect dimensions [16], we show in Sections IV and V of the Supplementary Material how the sampling schemes considered here for generalized MHS [Eq. (2)] and HS [Eq. (S2)] theory can be employed for several indirect chemical shift evolution periods of a multidimensional NMR experiments, or for any subset of jointly sampled chemical shift evolution periods of a GFT or RD [32] projection NMR experiment. The tensor product formation for **C**-vectors and **D**-matrices [see Eqs. (S40) and (S63a) of the Supplementary Material] implies that the conclusions drawn above for a single indirect dimension can be applied separately to several shift evolution periods, thereby rendering routine use straightforward also for spectra encoding higher dimensional (>2D) spectral information. The same holds if different sampling schemes are employed for different indirect evolution periods (see Section VI of the Supplementary Material).

For such spectra, the optimization of r.f. pulse sequence design and the choice of the best suited sampling scheme for CAM data acquisition is thus preferably accomplished independently for each indirect dimension. The same holds for GFT [17] and RD [32] projection NMR spectroscopy, where joint sampling of chemical shifts implies that phase corrections cannot be applied to individual evolution periods. Hence, it is advantageous to acquire, preferably for a test compound giving rise to signals with high S/N ratios distributed over the spectral ranges of interest, 2D planes in which only one of the several evolution periods is incremented in the indirect dimension.

The generalized theory of MHS enables one to design new NMR experiments in which the measurement of additional NMR parameters is encoded in secondary phase shifts or time domain amplitude imbalances. As an example, one can envisage to implement a 2D HNN(CO)CA experiment in which the polypeptide backbone $^{13}C^{\alpha}$ chemical shift of residue *i* is encoded in a secondary phase

shift of the ^{15}N shift evolution of the succeeding residue $i + 1$. This can be accomplished by using the r.f. pulse sequence of a 3D HNN(CO)CA experiment [3], and by setting the $^{13}C^{\alpha}$ shift evolution to a fixed delay of, for example, $1/(2 * \text{spectral width})$. Employing (c^{+}_{45}, c^{-}_{45})-MHS of ^{15}N chemical shifts, the secondary phase shift encodes the $^{13}C^{\alpha}$ shift and will lead for each peak in the 2D [^{15}N, ^{1}H] correlation spectrum to a corresponding quadrature image peak. The intensity ratio of the two peaks then allows one to measure the $^{13}C^{\alpha}$ shift relative to the r.f. pulse carrier position. Notably, the employment of DHMS offers the attractive option to edit the peaks and their quadrature images into different sub-spectra. This enables one to record the spectra without doubling the spectral width, thereby avoiding that off-resonance effects increase.

Overall, we expect that the generalized theory of HMS and HS presented here may greatly impact future data acquisition protocols for NMR spectroscopy, and possibly also for other areas where phase-sensitive pure-absorption mode time domain sampling is required.

Acknowledgment

This work was supported by the National Science Foundation (MCB 0817857 to T.S.).

Appendix A. Supplementary material

Supplementary data associated with this article can be found, in the online version, at doi:10.1016/j.jmr.2011.08.037.

References

[1] R.R. Ernst, G. Bodenhausen, A. Wokaun, Principles of Nuclear Magnetic Resonance in One and Two Dimensions, Clarendon Press, New York, 1987.
[2] N.E. Jacobsen, NMR Spectroscopy Explained: Simplified Theory, Applications and Examples for Organic Chemistry and Structural Biology, Wiley Interscience, Hoboken, NJ, 2007.
[3] J. Cavanagh, W.J. Fairbrother, A.G. Palmer III, M. Rance, N.J. Skelton, Protein NMR Spectroscopy, Academic Press, New York, 2007.
[4] D.J. States, R.A. Haberkorn, D.J. Ruben, A two-dimensional nuclear overhauser experiment with pure absorption phase in four quadrants, J. Magn. Reson. 48 (1982) 286–292.
[5] M.A. Delsuc, Spectral representation of 2D NNMR spectra by hypercomplex numbers, J. Magn. Reson. 77 (1988) 119–124.
[6] A.G. Redfield, S.D. Kunz, Quadrature Fourier NMR detection: simple multiplex for dual detection and discussion, J. Magn. Reson. 19 (1975) 250–254.
[7] G. Drobny, A. Pines, S. Sinton, D.P. Weitekamp, D. Wemmer, Fourier transform multiple quantum nuclear magnetic resonance, Faraday Div. Chem. Soc. Symp. 13 (1979) 49–55.
[8] G. Bodenhausen, R.L. Vold, R.R. Vold, Multiple quantum spin-echo spectroscopy, J. Magn. Reson. 37 (1980) 93–106.
[9] D. Marion, K. Wüthrich, Application of phase sensitive two-dimensional correlated spectroscopy (COSY) for measurements of ^{1}H–^{1}H spin–spin coupling constants in proteins, Biochem. Biophys. Res. Commun. 113 (1983) 967–974.
[10] Y. Wu, A. Ghosh, T. Szyperski, Clean absorption mode NMR data acquisition based on time-proportional phase incrementation, J. Struct. Funct. Genomics 10 (2009) 227–232.
[11] R.E. Hurd, Gradient-enhanced spectroscopy, J. Magn. Reson. 87 (1990) 422–428.
[12] J. Keeler, R.T. Clowes, A.L. Davis, E.D. Laue, Pulsed-field gradients: theory and practice, Methods Enzymol. 239 (1994) 145–207.
[13] A.G. Palmer, J. Cavanagh, R.A. Byrd, M. Rance, Sensitivity improvement in three-dimensional heteronuclear correlation NMR spectroscopy, J. Magn. Reson. 96 (1992) 416–424.
[14] L. Kay, P. Keifer, T. Saarinen, Pure absorption gradient enhanced heteronuclear single quantum correlation spectroscopy with improved sensitivity, J. Am. Chem. Soc. 114 (1992) 10663–10665.
[15] J. Schleucher, M. Sattler, C. Griesinger, Coherence selection by gradients without signal attenuation: application to the three-dimensional HNCO experiment, Angew. Chem. Int. Ed. Engl. 32 (1993) 1489–1491.
[16] Y. Wu, A. Ghosh, T. Szyperski, Clean absorption-mode NMR data acquisition, Angew. Chem. Int. Ed. Engl. 48 (2009) 1479–1483.
[17] S. Kim, T. Szyperski, GFT NMR, a new approach to rapidly obtain precise high-dimensional NMR spectral information, J. Am. Chem. Soc. 125 (2003) 1385–1393.
[18] S. Kim, T. Szyperski, GFT NMR experiments for polypeptide backbone and ^{13}Cbeta chemical shift assignment, J. Biomol. NMR 28 (2004) 117–130.
[19] H.S. Atreya, T. Szyperski, G-matrix Fourier transform NMR spectroscopy for complete protein resonance assignment, Proc. Natl. Acad. Sci. USA 101 (2004) 9642–9647.
[20] H.S. Atreya, A. Eletsky, T. Szyperski, Resonance assignment of proteins with high shift degeneracy based on 5D spectral information encoded in G2FT NMR experiments, J. Am. Chem. Soc. 127 (2005) 4554–4555.
[21] Y. Shen, H.S. Atreya, G. Liu, T. Szyperski, G-matrix Fourier transform NOESY-based protocol for high-quality protein structure determination, J. Am. Chem. Soc. 127 (2005) 9085–9099.
[22] A. Eletsky, H.S. Atreya, G. Liu, T. Szyperski, Probing structure and functional dynamics of (large) proteins with aromatic rings: L-GFT-TROSY (4,3)D HCCH NMR spectroscopy, J. Am. Chem. Soc. 127 (2005) 14578–14579.
[23] H.S. Atreya, E. Garcia, Y. Shen, T. Szyperski, J-GFT NMR for precise measurement of mutually correlated nuclear spin–spin couplings, J. Am. Chem. Soc. 129 (2007) 680–692.
[24] E. Kupce, R. Freeman, Projection-reconstruction technique for speeding up multidimensional NMR spectroscopy, J. Am. Chem. Soc. 126 (2004) 6429–6440.
[25] S. Hiller, F. Fiorito, K. Wuthrich, G. Wider, Automated projection spectroscopy (APSY), Proc. Natl. Acad. Sci. USA 102 (2005) 10876–10881.
[26] H.R. Eghbalnia, A. Bahrami, M. Tonelli, K. Hallenga, J.L. Markley, High-resolution iterative frequency identification for NMR as a general strategy for multidimensional data collection, J. Am. Chem. Soc. 127 (2005) 12528–12536.
[27] H.R. Eghbalnia, A. Bahrami, L. Wang, A. Assadi, J.L. Markley, Probabilistic identification of spin systems and their assignments including coil–helix inference as output (PISTACHIO), J. Biomol. NMR 32 (2005) 219–233.
[28] K. Nagayama, Four-quadrant pure-phase representation of two-dimensional spectra with time-reversal or frequency inversion, J. Magn. Reson. 66 (1986) 240–249.
[29] P. Bachmann, W.P. Aue, L. Müller, R.R. Ernst, Phase separation in two-dimensional spectroscopy, J. Magn. Reson. 28 (1977) 29–39.
[30] J.C. Hoch, A.S. Stern, NMR Data Processing, Wiley-Liss, New York, 1996.
[31] G. Zhu, D.A. Torchia, A. Bax, Discrete Fourier transformation of NMR signals. The relationship between sampling delay time and spectral baseline, J. Magn. Reson. A105 (1993) 219–222.
[32] T. Szyperski, D.C. Yeh, D.K. Sukumaran, H.N. Moseley, G.T. Montelione, Reduced-dimensionality NMR spectroscopy for high-throughput protein resonance assignment, Proc. Natl. Acad. Sci. USA 99 (2002) 8009–8014.
[33] D.M. Parish, T. Szyperski, Simultaneously cycled NMR spectroscopy, J. Am. Chem. Soc. 130 (2008) 4925–4933.
[34] A. Schweiger, G. Jeschke, Principles of Pulse Electron Paramagnetic Resonance, Oxford University Press, Oxford, UK; New York, 2001.
[35] D.I. Hoult, R.E. Richards, Critical factors in the design of sensitive high resolution nuclear magnetic resonance spectrometers, Proc. Roy. Soc. Lond. A 344 (1975) 311–340.